

Yttrium Iron Garnet Thin Films with Very Low Damping Obtained by Recrystallization of Amorphous Material

C. Hauser,¹ T. Richter,¹ N. Homonnay,¹ C. Eisenschmidt,¹
H. Deniz,² D. Hesse,² S. Ebbinghaus,³ and G. Schmidt^{1,4,*}

¹*Institute of Physics, Martin-Luther-Universität Halle-Wittenberg,
Von-Danckelmann-Platz 3, D-06120 Halle, Germany*

²*Max-Planck-Institut für Mikrostrukturphysik,
Weinberg 2, D-06120 Halle, Germany*

³*Institute of Chemistry, Martin-Luther-Universität Halle-Wittenberg,
Kurt-Mothes-Str. 2, D-06120 Halle, Germany*

⁴*Interdisziplinäres Zentrum für Materialwissenschaften,
Martin-Luther University Halle-Wittenberg, Nanotechnikum Weinberg,
Heinrich-Damerow-Str. 4, D-06120 Halle, Germany*

Abstract

We have investigated recrystallization of amorphous Yttrium Iron Garnet (YIG) by annealing in oxygen atmosphere. Our findings show that well below the melting temperature the material transforms into a fully epitaxial layer with exceptional quality, both structural and magnetic. In ferromagnetic resonance (FMR) ultra low damping and extremely narrow linewidth can be observed. For a 56 nm thick layer a damping constant of $\alpha = (6.63 \pm 1.50) \cdot 10^{-5}$ is found and the linewidth at 9.6 GHz is as small as 1.30 ± 0.05 Oe which are the lowest values for PLD grown thin films reported so far. Even for a 20 nm thick layer a damping constant of $\alpha = (7.51 \pm 1.40) \cdot 10^{-5}$ is found which is the lowest value for ultrathin films published so far. The FMR linewidth in this case is 3.49 ± 0.10 Oe at 9.6 GHz. Our results not only present a method of depositing thin film YIG of unprecedented quality but also open up new options for the fabrication of thin film complex oxides or even other crystalline materials.

I. INTRODUCTION

YIG can be considered the most prominent material in spin dynamics in thin films and related areas. It is widely used in ferromagnetic resonance experiments¹⁻⁶, research on magnonics⁷⁻¹⁴ and magnon-based Bose-Einstein-condensates¹⁵⁻¹⁸ because of its exceptionally low damping even in thin films. In research on spin pumping¹⁹⁻²³ and investigation of the inverse spin hall effect^{1,19,24-27} it greatly facilitates experiments because it is an insulating material which avoids numerous side effects which occur when ferromagnetic metals are used.^{28,29} The field of spin caloritronics³⁰⁻³⁸ also would not have developed that rapidly without the availability of a non-conducting magnet with long magnon lifetimes.

The new fields of applications have resulted in a growing need of high quality thin films, for example for integrated magnonics where layers need to be as thin as 100 nm or even less. While formerly only micrometer thick films were used which can be obtained by liquid phase epitaxy with very high quality³⁹⁻⁴² ultrathin films are nowadays mostly fabricated by pulsed laser deposition (PLD) of epitaxial films at elevated temperature. Especially for ultra thin films (20 nm or less) grown by PLD quality is high but limited and best results so far show a linewidth in FMR of 2.1 Oe at 9.6 GHz.¹

II. SAMPLE FABRICATION

The amorphous YIG layers are deposited on (111) oriented gallium gadolinium garnet (GGG) substrates. After deposition the samples are removed from the PLD chamber and cut into smaller pieces before the subsequent annealing procedure which is done in a quartz oven under pure (99.998 %) oxygen atmosphere at ambient pressure at 800°C for 30 minutes (sample A, 56 nm thick), at 800°C for three hours (sample B, 20 nm thick), and at 900°C for four hours (sample C, 113 nm thick). After annealing the samples are subject to various structural and magnetic characterization experiments.

III. STRUCTURAL CHARACTERIZATION

Structural characterization is done by X-ray diffraction, X-ray reflectometry transmission electron microscopy, and Reflection high energy electron diffraction (RHEED).

A. X-ray characterization

X-ray diffraction is performed by doing an $\omega/2\theta$ scan of the (444) reflex and a rocking curve of the YIG layer peak. Before annealing the diffraction pattern (Figure 1a) only shows the peak of the GGG substrate indicating an amorphous or at least highly polycrystalline YIG film. A truly amorphous nature is confirmed by transmission electron microscopy as described below. After annealing, the diffraction pattern is completely changed. Figure 1b shows the $\omega/2\theta$ scan for sample C. Here we clearly observe the diffraction peak of the YIG film at an angle corresponding to the small lattice mismatch of YIG on GGG which is only 0.057%. Even thickness fringes can be observed indicating a very smooth layer with low interface and surface roughness. The layer peak is further investigated in a rocking curve (Figure 1c) which shows a full width at half maximum (FWHM) of 0.015° indicating a fully pseudomorphic YIG layer. Roughness is also crosschecked using X-ray reflectometry showing an RMS value of less than 0.2 nm^{43} . It should, however, be noted that for not-annealed layers the RMS roughness is even smaller than 0.1 nm .

B. Transmission electron microscopy

For Transmission electron microscopy (TEM) preparation the sample surface is protected by depositing a thin Pt layer. Then thin lamellae are cut out using focused ion beam preparation. The orientation of the samples is chosen for cross sectional TEM along the cubic crystalline axis. TEM is performed using a JEOL JEM-4010 electron microscope at an acceleration voltage of 400 kV. For the nominally amorphous sample the pictures (Figure 2a) show a pure film without inclusions but also without any trace of polycrystallinity. Further analysis using fast fourier transform confirms that the YIG layer is indeed completely amorphous. For an annealed sample (sample C) the result of the TEM investigation is surprising (Figure 2b). The sample is not only monocrystalline but it also shows no sign of inclusions or defects and even the interface to the GGG appears flawless.

C. Reflection high energy electron diffraction

The atomic order of the layer surface after annealing is further investigated by Reflection high energy electron diffraction (RHEED). For this purpose sample B is again introduced

into the PLD chamber after the annealing process. After evacuation a clear RHEED pattern is observed. The RHEED image (Figure 2c) not only shows the typical pattern for a YIG surface during high temperature growth but also exhibits the so called Kikuchi lines.⁴⁴ We do not observe these lines in high temperature growth of epitaxial YIG. They are typically a sign of a surface of excellent two dimensional growth, again indicating that the crystalline quality of the annealed layers is extremely high.

IV. MAGNETIC CHARACTERIZATION

Magnetic characterization is done using SQUID magnetometry and FMR at room temperature.

A. SQUID magnetometry

In SQUID magnetometry hysteresis loops are taken on sample C. The data is corrected by subtracting a linear paramagnetic contribution which is caused by the GGG substrate. After correction the observed saturation magnetization is $(105 \pm 3) \text{ emu cm}^{-3}$ which is approx. 30% below the bulk value⁴⁵ (Figure 3). The coercive field is determined as $(0.8 \pm 0.1) \text{ Oe}$.

B. Ferromagnetic resonance

FMR is performed by putting the samples face down on a coplanar waveguide whose magnetic radio frequency (RF) field is used for excitation. The setup is placed in a homogeneous external magnetic field which is superimposed with a small low frequency modulation. RF absorption is measured using a lock-in amplifier. As expected no signal can be detected for unannealed YIG layers. For annealed samples a clear resonance is observed. Figure 4a shows the resonance signal for sample A. The linewidth which is obtained by multiplying the peak to peak linewidth of the derivative of the absorption by a factor of $\sqrt{3}/2^{2,3,46,47}$ is only $1.30 \pm 0.05 \text{ Oe}$ at 9.6 GHz which is the smallest value for thin films reported so far.¹ In Figure 4b the resonance of sample B is shown. Here the linewidth at 9.6 GHz is $3.49 \pm 0.10 \text{ Oe}$. For sample C the linewidth is $1.65 \pm 0.10 \text{ Oe}$ at 9.6 GHz (no figure).

In order to determine the damping constant α frequency dependent measurements are per-

formed on sample A. The excitation frequency is varied between 8 and 12 GHz. Results are plotted in Figure 4c. As described by Chang *et al.*⁴⁶ and Liu *et al.*² we first determine the gyromagnetic ratio of $\gamma = (2.92 \pm 0.01) \text{ MHz Oe}^{-1}$ and a linewidth at zero magnetic field of approx. $1.11 \pm 0.05 \text{ Oe}$. The damping can then be calculated from the frequency dependence of the linewidth to $\alpha = (6.63 \pm 1.50) \cdot 10^{-5}$. This damping is even lower than the lowest value reported by Chang *et al.*⁴⁶. It is interesting to note that Chang *et al.* did not observe a similarly small linewidth for their layer.⁴⁶ dAllivy Kelly *et al.* on the other hand do observe a smaller linewidth for 20 nm thick layers of 2.1 Oe at 9.6 GHz¹, however, the damping they find is three times as big as in our case. For sample B (20 nm) we found a gyromagnetic ratio of $\gamma = (2.81 \pm 0.01) \text{ MHz Oe}^{-1}$ and a linewidth at zero magnetic field of approx. $3.25 \pm 0.05 \text{ Oe}$ and the damping was determined as $\alpha = (7.51 \pm 1.40) \cdot 10^{-5}$ which is also lower than any other value reported for similarly thin films (Figure 4d).

V. DISCUSSION

In conclusion we can state that using high temperature annealing in oxygen atmosphere it is possible to transform amorphous YIG layers of tens of nanometers of thickness into epitaxial thin films with extremely small FMR linewidth and exceptionally low damping. The crystalline quality is extremely high. Our findings may thus present a new and easy route for thin film fabrication of epitaxial complex oxides.

VI. METHODS

The substrates are prepared by cleaning in acetone and isopropanol and then introduced into the PLD chamber which is copper sealed and UHV compatible with a background pressure as low as 10^{-9} mbar. Deposition is done at an oxygen partial pressure of 0.025 mbar with the substrate at room temperature. A laser with a typical fluency of 2.5 J cm^{-2} and a wavelength of 248 nm is used at a repetition rate of 5 Hz. The target is a stoichiometric YIG target prepared in-house. With these parameters we obtain a growth rate of approx. 0.5 nm min^{-1} .

Acknowledgements

This work was supported by the European Commission in the project IFOX under grant agreement NMP3-LA-2010-246102 and by the DFG in the SFB 762. We thank Georg Woltersdorf and Sergey Manuilov for fruitful discussion.

-
- * Correspondence to G. Schmidt: georg.schmidt@physik.uni-halle.de
- ¹ d’Allivy Kelly, O. *et al.* Inverse spin hall effect in nanometer-thick yttrium iron garnet/pt system. *Appl. Phys. Lett.* **103**, 082408 (2013).
- ² Liu, T. *et al.* Ferromagnetic resonance of sputtered yttrium iron garnet nanometer films. *J. Appl. Phys.* **115**, 17A501 (2014).
- ³ Sun, Y. *et al.* Growth and ferromagnetic resonance properties of nanometer-thick yttrium iron garnet films. *Appl. Phys. Lett.* **101**, 152405 (2012).
- ⁴ Sun, Y. *et al.* Damping in yttrium iron garnet nanoscale films capped by platinum. *Phys. Rev. Lett.* **111**, 106601 (2013).
- ⁵ Manuilov, S. A. & Grishin, A. M. Pulsed laser deposited yig films: Nature of magnetic anisotropy ii. *J. Appl. Phys.* **108**, 013902 (2010).
- ⁶ Manuilov, S. A., Khartsev, S. I. & Grishin, A. M. Pulsed laser deposited yig films: Nature of magnetic anisotropy i. *J. Appl. Phys.* **106**, 123917 (2009).
- ⁷ Chumak, A. V., Serga, A. A. & Hillebrands, B. Magnon transistor for all-magnon data processing. *Nat. Commun.* **5**, 4700 (2014).
- ⁸ Kurebayashi, H. *et al.* Controlled enhancement of spin-current emission by three-magnon splitting. *Nat. Mat.* **10**, 660–664 (2011).
- ⁹ Ustinov, A. B., Drozdovskii, A. V. & Kalinikos, B. A. Multifunctional nonlinear magnonic devices for microwave signal processing. *Appl. Phys. Lett.* **96**, 142513 (2010).
- ¹⁰ Inoue, M. *et al.* Investigating the use of magnonic crystals as extremely sensitive magnetic field sensors at room temperature. *Appl. Phys. Lett.* **98**, 132511 (2011).
- ¹¹ Yu, H. *et al.* Magnetic thin-film insulator with ultra-low spin wave damping for coherent nanomagnonics. *Sci. Rep.* **4**, 6848 (2014).
- ¹² Bi, K. *et al.* Magnetically tunable mie resonance-based dielectric metamaterials. *Sci. Rep.* **4**,

- 7001 (2014).
- ¹³ Demokritov, S. O. *et al.* Experimental observation of symmetry-breaking nonlinear modes in an active ring. *Nature* **426**, 159–162 (2003).
 - ¹⁴ Chumak, A. V. *et al.* All-linear time reversal by a dynamic artificial crystal. *Nat. Commun.* **1**, 141 (2010).
 - ¹⁵ Li, F., Saslow, W. M. & Pokrovsky, V. L. Phase diagram for magnon condensate in yttrium iron garnet film. *Sci. Rep.* **3** (2013).
 - ¹⁶ Nowik-Boltyk, P., Dzyapko, O., Demidov, V. E., Berloff, N. G. & Demokritov, S. O. Spatially non-uniform ground state and quantized vortices in a two-component bose-einstein condensate of magnons. *Sci. Rep.* **2** (2012).
 - ¹⁷ Demokritov, S. O. *et al.* Bose-einstein condensation of quassi-equilibrium magnons at room temperature under pumping. *Nature* **443**, 430–433 (2006).
 - ¹⁸ Serga, A. A. *et al.* Bose-einstein condensation in an ultra-hot gas of pumped magnons. *Nat. Commun.* **5** (2014).
 - ¹⁹ Ando, K., Watanabe, S., Mooser, S., Saitoh, E. & Siringhaus, H. Solution-processed organic spin-charge converter. *Nat. Mat.* **12**, 622–627 (2013).
 - ²⁰ Burrowes, C. *et al.* Enhanced spin pumping at yttrium iron garnet/au interfaces. *Appl. Phys. Lett.* **100**, 092403 (2012).
 - ²¹ Jungfleisch, M. B., Lauer, V., Neb, R., Chumak, A. V. & Hillebrands, B. Improvement of the yttrium iron garnet/platinum interface for spin pumping-based applications. *Appl. Phys. Lett.* **103**, 022411 (2013).
 - ²² Rezende, S. M. *et al.* Enhanced spin pumping damping in yttrium iron garnet/pt bilayers. *Appl. Phys. Lett.* **102**, 012402 (2013).
 - ²³ Žutić, I. & Dery, H. Spintronics: Taming spin currents. *Nat. Mat.* **10**, 647–648 (2011).
 - ²⁴ Sakimura, H., Tashiro, T. & Ando, K. Nonlinear spin-current enhancement enabled by spin-damping tuning. *Nat. Commun.* **5**, 5730 (2014).
 - ²⁵ Castel, V., Vlietstra, N., Ben Youssef, J. & van Wees, B. J. Platinum thickness dependence of the inverse spin-hall voltage from spin pumping in a hybrid yttrium iron garnet/platinum system. *Appl. Phys. Lett.* **101**, 132414 (2012).
 - ²⁶ Schreier, M. *et al.* Sign of inverse spin hall voltages generated by ferromagnetic resonance and temperature gradients in yttrium iron garnet platinum bilayers. *J. Phys. D: Appl. Phys.* **48**,

- 025001 (2015).
- ²⁷ Kajiwara, Y. *et al.* Transmission of electrical signals by spin-wave interconversion in a magnetic insulator. *Nature* **464**, 262–266 (2010).
- ²⁸ Obstbaum, M. *et al.* Inverse spin hall effect in $\text{ni}_{81}\text{fe}_{19}$ /normal-metal bilayers. *Phys. Rev. B* **89** (2014).
- ²⁹ Mecking, N., Gui, Y. S. & Hu, C.-M. Microwave photovoltage and photoresistance effects in ferromagnetic microstrips. *Phys. Rev. B* **76** (2007).
- ³⁰ Bauer, G. E. W., Saitoh, E. & van Wees, B. J. Spin caloritronics. *Nat. Mat.* **11**, 391–399 (2012).
- ³¹ Sinova, J. Spin seebeck effect: Thinks globally but acts locally. *Nat. Mat.* **9**, 880–881 (2010).
- ³² Kirihara, A. *et al.* Spin-current-driven thermoelectric coating. *Nat. Mat.* **11**, 686–689 (2012).
- ³³ Siegel, G., Prestgard, M. C., Teng, S. & Tiwari, A. Robust longitudinal spin-seebeck effect in bi-yig thin films. *Sci. Rep.* **4** (2014).
- ³⁴ Qu, D., Huang, S., Hu, J., Wu, R. & Chien, C. Intrinsic spin seebeck effect in au/yig . *Phys. Rev. Lett.* **110** (2013).
- ³⁵ An, T. *et al.* Unidirectional spin-wave heat conveyer. *Nat. Mat.* **12**, 549–553 (2013).
- ³⁶ Uchida, K.-i. *et al.* Observation of longitudinal spin-seebeck effect in magnetic insulators. *Appl. Phys. Lett.* **97**, 172505 (2010).
- ³⁷ Adachi, H., Ohe, J.-i., Takahashi, S. & Maekawa, S. Linear-response theory of spin seebeck effect in ferromagnetic insulators. *Phys. Rev. B* **83** (2011).
- ³⁸ Agrawal, M. *et al.* Direct measurement of magnon temperature: New insight into magnon-phonon coupling in magnetic insulators. *Phys. Rev. Lett.* **111** (2013).
- ³⁹ Görnert, P. *et al.* Growth kinetics and some properties of thick lpe yig layers. *J. Cryst. Growth* **87**, 331–337 (1988).
- ⁴⁰ Wei Hongxu & Wang Wenshu. The growth of lpe yig films with narrow fmr linewidth. *IEEE T. Magn.* **20**, 1222–1223 (1984).
- ⁴¹ Čermák, J., Abrahám, A., Fabián, T., Kaboš, P. & Hyben, P. Yig based lpe films for microwave devices. *J. Magn. Magn. Mater.* **83**, 427–429 (1990).
- ⁴² Yong Choi, D. & Jin Chung, S. Annealing behaviors of lattice misfit in yig and la-doped yig films grown on ggg substrates by lpe method. *J. Cryst. Growth* **191**, 754–759 (1998).
- ⁴³ Lang, M. *et al.* Proximity induced high-temperature magnetic order in topological insulator - ferrimagnetic insulator heterostructure. *Nano Lett.* **14**, 3459–3465 (2014).

- ⁴⁴ Braun, W. *Applied RHEED: Reflection high-energy electron diffraction during crystal growth*, vol. 154 of *Springer tracts in modern physics* (Springer, Berlin and New York, 1999).
- ⁴⁵ Hansen, P. Saturation magnetization of gallium-substituted yttrium iron garnet. *J. Appl. Phys.* **45**, 2728 (1974).
- ⁴⁶ Houchen Chang *et al.* Nanometer-thick yttrium iron garnet films with extremely low damping. *IEEE Magn. Lett.* **5**, 6700104 (2014).
- ⁴⁷ Georg Woltersdorf. *Spin-Pumping and Two-Magnons Scattering in Magnetic Multilayers*. Ph.D. thesis, Simon Fraser University, Vancouver (August 2004).

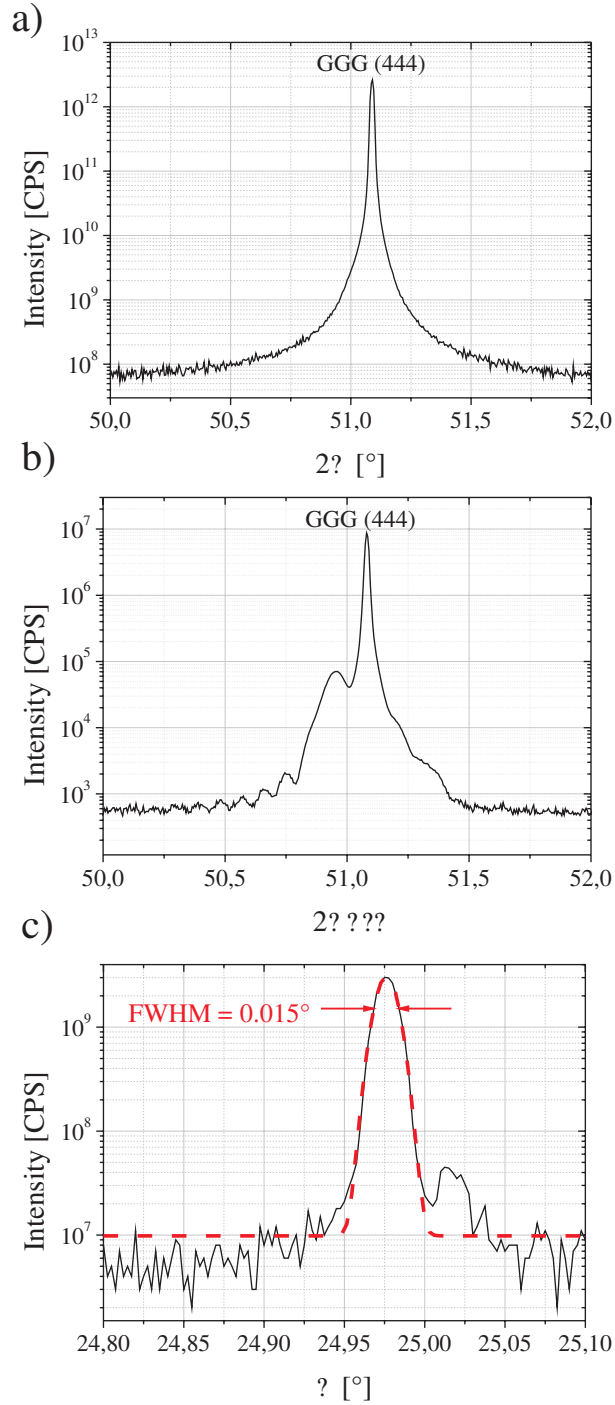


FIG. 1: X-ray diffraction ($\omega/2\theta$ scans) for an unannealed (a) and an annealed YIG layer (b). Before annealing only the substrate peak is visible. After annealing the YIG peak clearly shows up. The position of the peak and the thickness fringes indicate fully pseudomorphic growth and smooth interfaces. (c) shows a rocking curve of the layer peak shown in (b). The full width at half maximum is only 0.015° . The dotted line shows a Gaussian fit to the peak.

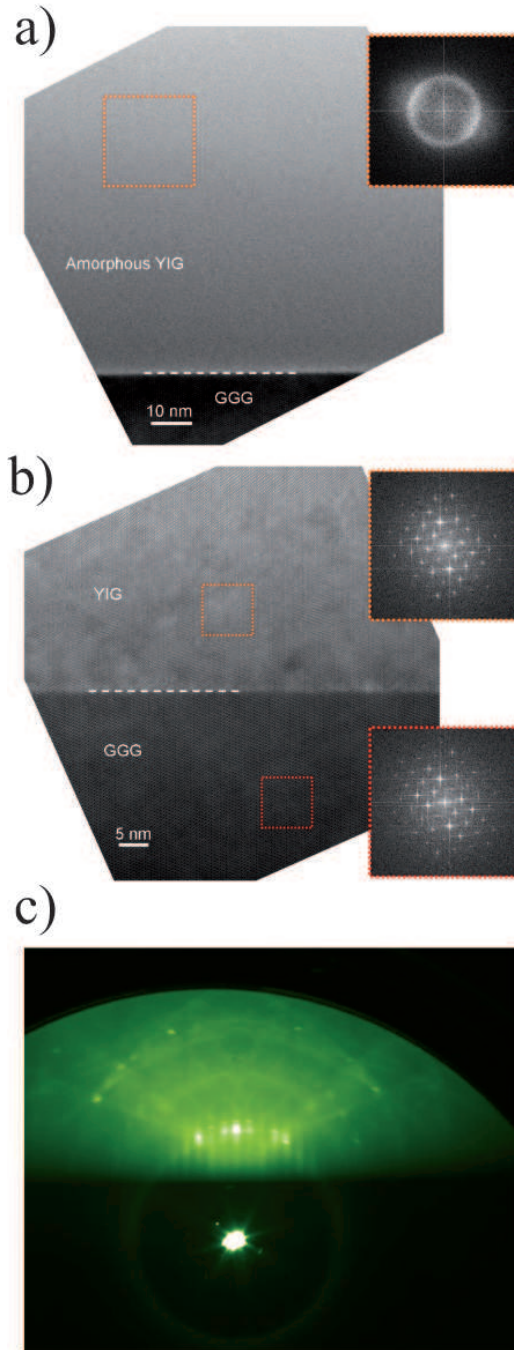


FIG. 2: a) A high resolution TEM (HRTEM) image of an amorphous YIG film on GGG substrate. The inset shows a FFT pattern from the region of interest (dotted frame) in the amorphous layer. b) A HRTEM image of the interface between the annealed YIG film and the GGG substrate of sample C. The insets show FFT patterns from the regions of interest in the film and the substrate. The YIG film exhibits epitaxial growth with respect to the substrate and appears monocrystalline. c) RHEED image obtained from the surface of an annealed YIG film (sample B). Kikuchi lines⁴⁴ indicate a two dimensional highly ordered surface.

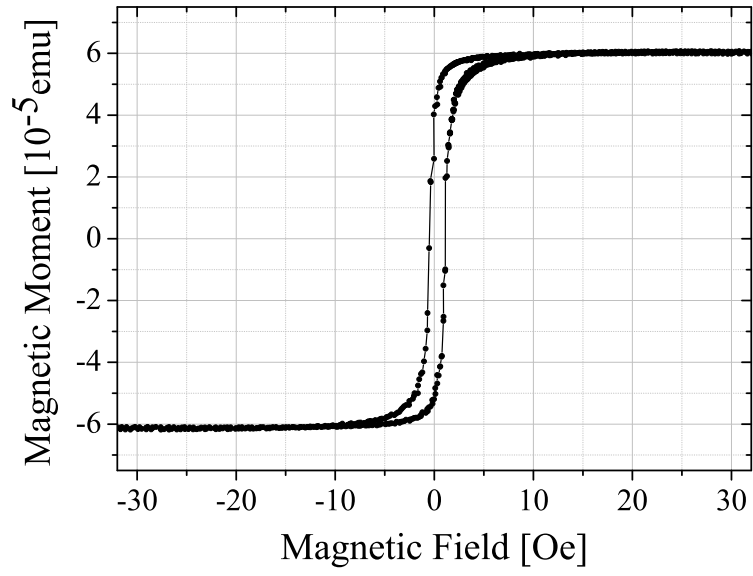


FIG. 3: Hysteresis loop as measured by SQUID magnetometry for a 113 nm thick YIG sample after annealing. The paramagnetic background caused by the GGG substrate was subtracted.

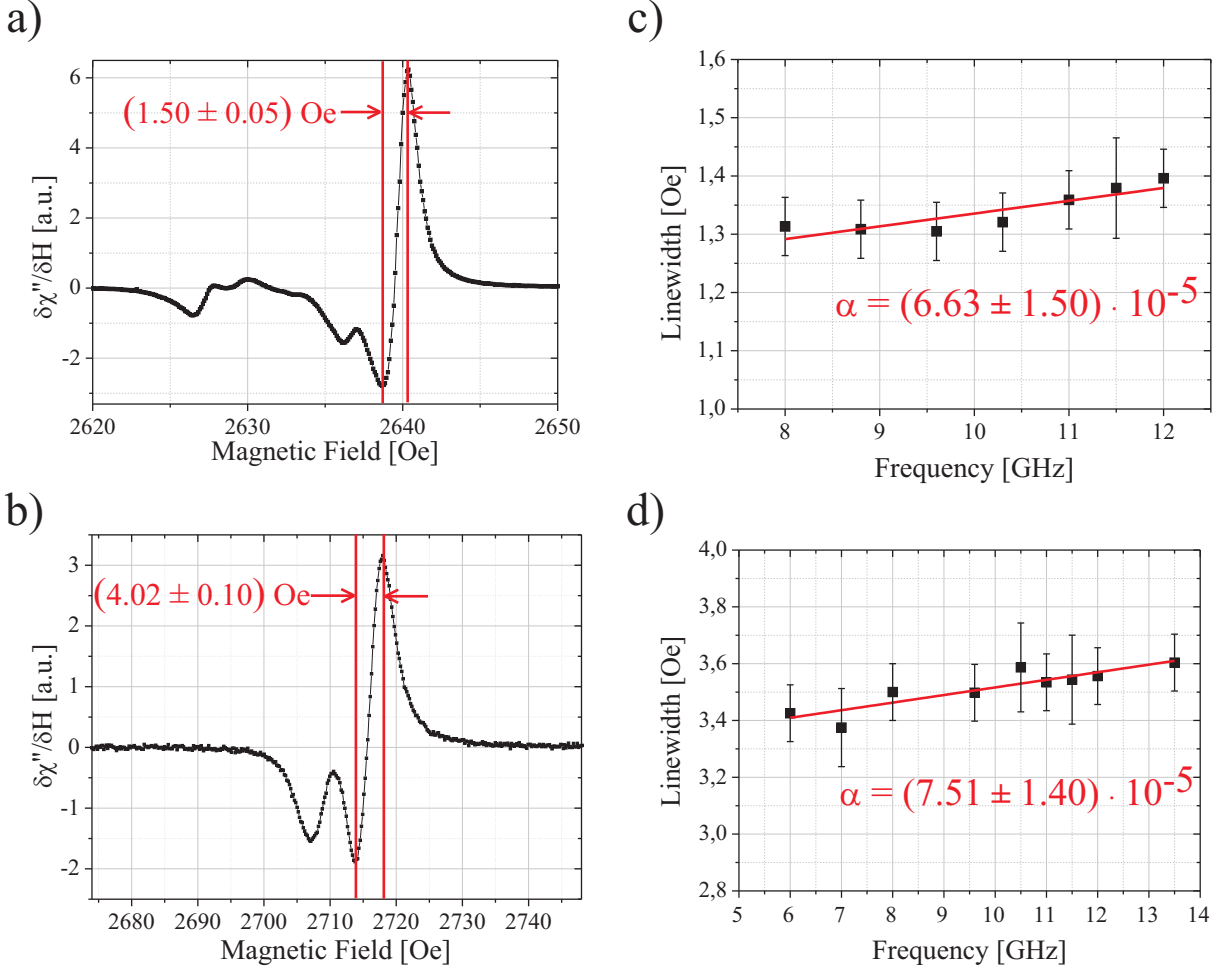


FIG. 4: a) and b) FMR data obtained at 9.6 GHz for a 56 nm thick (a, sample A) and a 20 nm thick (b, sample B) YIG layer after annealing. The main resonance lines have a peak-to-peak linewidth of 1.51 ± 0.05 Oe (sample A) and 4.02 ± 0.10 Oe (sample B). This peak-to-peak linewidth corresponds to a true linewidth of 1.30 ± 0.05 Oe and 3.49 ± 0.10 Oe, respectively. c) and d) Frequency dependence of the FMR linewidth for sample A and sample B. The fits are a straight line corresponding to a damping of $\alpha = (6.63 \pm 1.50) \cdot 10^{-5}$ (c, sample A) and $\alpha = (7.51 \pm 1.40) \cdot 10^{-5}$ (d, sample B).